



**HAL**  
open science

## Experimental observation on a laterally loaded pile in unsaturated silty soil

Leonardo Lalicata, Augusto Desideri, Francesca Casini, Luc Thorel

► **To cite this version:**

Leonardo Lalicata, Augusto Desideri, Francesca Casini, Luc Thorel. Experimental observation on a laterally loaded pile in unsaturated silty soil. *Canadian Geotechnical Journal*, 2018, 35p. 10.1139/cgj-2018-0322 . hal-01945314

**HAL Id: hal-01945314**

**<https://hal.science/hal-01945314>**

Submitted on 5 Dec 2018

**HAL** is a multi-disciplinary open access archive for the deposit and dissemination of scientific research documents, whether they are published or not. The documents may come from teaching and research institutions in France or abroad, or from public or private research centers.

L'archive ouverte pluridisciplinaire **HAL**, est destinée au dépôt et à la diffusion de documents scientifiques de niveau recherche, publiés ou non, émanant des établissements d'enseignement et de recherche français ou étrangers, des laboratoires publics ou privés.

1 **Experimental observation on a laterally loaded pile in**  
2 **unsaturated silty soil**

3 L.M. Lalicata & A. Desideri

4 *Dipartimento di Ingegneria strutturale e geotecnica. Sapienza Università di Roma. Rome, Italy.*

5 F. Casini

6 *Dipartimento di Ingegneria Civile e Ingegneria Informatica, Università degli Studi di Roma "Tor Vergata",*  
7 *Rome, Italy.*

8 L. Thorel

9 *IFSTTAR, GERS Department, Geomaterials and Modelling in Geotechnics Laboratory, Bouguenais, France.*

10

11

**Abstract:** An experimental study has been carried out to investigate the effects of soil partial saturation on the behaviour of laterally loaded piles. The proposed study has been conducted by means of centrifuge tests at  $100\times g$ , where a single vertical pile has been subjected to a combination of static horizontal load and bending moment. The study has been conducted on a silty soil characterized with laboratory testing under saturated and unsaturated conditions. During flight, two different positions of water table have been explored. The influence of density has been investigated compacting the sample with two different void ratio. Finally, the effects of a variation of saturation degree on the pile response under loading have been studied rising the water table to ground surface. Data interpretation allows drawing different considerations on the effects of partial saturation on the behaviour of laterally loaded piles. As expected, compared to saturated soils, partial saturation leads always to a stiffer and resistant response of the system. However, the depth of the maximum bending moment is related to the position of water table and the bounding effects induced by partial saturation appears to be more important for loose soils.

**Key words:** Centrifuge modelling; unsaturated soils; soil-structure interaction; piles; lateral loading

12

## 13 Introduction

14 The significant soil volume interested by the kinematics of piles foundation under lateral loading  
15 is typically limited vertically in the first meters (several diameters of pile) of depth from ground level.  
16 A number of studies available in literature (Banerjee and Davies, 1978; Randolph, 1981; Krishnan et  
17 al.,1983 Higgins et al., 2013, Di Laora and Rovithis, 2015) point out that, in this class of problems,  
18 the system response is mainly influenced by relative pile soil stiffness ratio, opportunely evaluated in  
19 the significant volume of soil, while for short and rigid piles response is affected both by stiffness  
20 and slenderness ratio. Most relevant parameters such as head displacement and rotation, maximum  
21 bending moment and its position along pile length are also strongly influenced by non-linear stress-  
22 strain relationships of soils (Budhu & Davies 1987, 1987; Russo, 2016).

23 The behaviour of pile under lateral loading depending, among others factors, from the stiffness  
24 of the pile and of the soil surroundings. It is well known that a flexible (or long) pile is characterized  
25 by no variation of load or displacement at the tip level during lateral loading at the head. While, a  
26 perfectly rigid (or short) pile should behaves with a constant rotation all along its length. The reality  
27 is often in between those idealised two extremes cases.

28 In many applications, the significant volume of soil can be above the water table, hence in partial  
29 saturation conditions. Nowadays, the effects of suction and saturation degree on the mechanical  
30 behaviour of soils have been widely investigated by laboratory studies (Fredlund et al 1978; Cui &  
31 Delage 1996; Escario & Saez, 1986; Vassallo et al., 2007; Casini, 2008; Casini et al., 2012; Biglari *et al.*,  
32 2011; Sivakumar and Wheeler 2000; Salager et al 2013, Hamid & Miller 2009). In the last years, some  
33 studies have been published on the influence of partial saturation in engineering problems such us  
34 bearing capacity of shallow and deep foundations (Georgiadis *et al* 2003; Vanapalli 2009). However,  
35 in soil-structure interaction problem, potential benefits of suction are often neglected by practical  
36 applications.

37 Physical centrifuge modelling represents a valid methodology to experimentally investigate soil-  
38 structure interaction problems. The small scale model is linked to the full scale prototype, following  
39 scaling laws (e.g. Corté, 1989; Schofield ,1990 ). When the scale of the model is  $1/N$ , the model has

40 to be subjected to a centrifuge  $g$ -level of  $N$ . Studies were so far conducted on fully saturated or  
41 completely dried soil model. Only recently, due to a better understanding of the behaviour of  
42 compacted soils (Thorel *et al.*, 2011; Caicedo *et al.*, 2014) for the preparation of soil model and to the  
43 new instrumentation available to measure suction and saturation degree during the tests (Caicedo and  
44 Thorel, 2014; Soranzo *et al.*, 2015), unsaturated soil behaviour has been explored by centrifuge  
45 modelling (Casini 2008, Thorel *et al.*, 2011, Soranzo *et al.*, 2015). Scaling laws for unsaturated soils  
46 have been experimentally investigated by Depountis *et al.* (2001) and Caicedo *et al.* (2006). The authors  
47 found that capillary rise and diffusion time in the centrifuge could be scaled of  $1/N$  and  $1/N^2$   
48 respectively. Details of analytical formulation can be found in Caicedo and Thorel (2014) and Soranzo  
49 *et al.* (2015). The scaling factors adopted in this study are listed in Table 1

50 The current experimental study is focused on the influence of partial saturation on the behaviour  
51 of laterally loaded pile. The aim of the experiment is to study the response of a single vertical free-  
52 head pile, embedded in a homogenous fine graded soil, subjected to a combination of lateral loading  
53 and bending moment, under different hydraulic condition and initial void ratio. The study has been  
54 developed by means of physical modelling in macro-gravity ( $N=100\times g$ ) using the IFSTTAR  
55 centrifuge facilities of Nantes (Rosquoët *et al* 2007).

56 The study is organized as follows. First, model and instrumentation set up are reported. Secondly,  
57 the soil hydro-mechanical characterization is briefly presented together with the results of flooding  
58 test in oedometer apparatus conducted to explore volumetric behaviour during wetting. Thirdly, soil  
59 model preparation and test procedures are presented and described. Finally, the results of the study  
60 are discussed focusing the attention on the load-head displacement relationship and flexural pile  
61 response, exploring the influence of the different structure and soil saturation conditions. In the last  
62 section, the effects of a variation of saturation degree on the pile behaviour are analysed.

## 63 **Experimental facilities**

### 64 SOIL PROPERTIES

65 The material used is a commercial kaolin named B-Grade kaolin. The soil has a fine silt fraction  
66 of about 90% and a clay fraction of 10%. As reported in Table 2, the material has a liquid limit ( $w_L$ )

67 of 42%, a plastic limit ( $w_p$ ) of 28% and therefore a plastic index (IP) of 14%. The main hydro-  
68 mechanical saturated parameters are summarized in Table 2.

69 In order to define the after compaction conditions ( $w$ ,  $e$ ) for centrifuge models, a number of  
70 flooding experiments have been performed on samples with different compaction features with a  
71 constant vertical stress  $\sigma_v=150$  kPa. This load corresponds approximately to the vertical stress  
72 exerted at half of pile embedded length ( $z \cong 8$ m).

73 Tests are carried out in oedometric apparatus of 70 mm in diameter and 18 mm thick. Following  
74 the standard procedure proposed by several authors (Wheeler & Sivakumar, 1995; Tarantino & De  
75 Col; 2008), the soil has been preliminarily dried at 105 °C for 24 hours then demineralized water has  
76 been added to reach the desired water content. The material has been kept in sealed bags for 24-48  
77 hours. The specimens have been statically compacted ( $v=1.5$  mm/min) directly in the oedometric  
78 ring, allowing to reach quite accurately the required void ratio.

79 The tests consist of two steps:

- 80 • Load at constant water content;
- 81 • Soaking at constant load;

82 The grid of water content and void ratio has been chosen on the base of the results of the Standard  
83 Proctor test, black line in Figure 1, from which results an optimum water content ( $w_{opt}$ ) of 0.21 and  
84 an optimum void ratio ( $e_{opt}$ ) of 0.74 (optimum dry density  $\gamma_{d,opt}=1.528$  gr/cm<sup>3</sup>). Three voids ratio are  
85 taken into account ( $e_0 = 0.77, 0.92$  and  $1.12$ ), for water content ranging from 10% to 26%, with steps  
86 of 4 %, in order to cover both *dry* than *wet side* of the Proctor curve, Figure 1. For each grid point at  
87 least two samples are tested.

88 Moreover, samples conditions after soaking, are presented in Figure 1 with grey symbols, grouped  
89 for initial void ratio. All the samples have elevated values of saturation degree, from 0.95 to 1.0. A  
90 significant influence of initial void ratio can be recognized: more compacted ( $e_0=0.77$ ) soil shows a  
91 little swelling during wetting while the others exhibit collapse deformation during soaking increasing

92 with initial void ratio. A negligible influence of compaction water content on the deformation upon  
93 wetting has been found for this material.

94 Based on the experimental results obtained, reported in Figure 1, in order to have a collapsible  
95 and a swelling soil sample upon wetting, two initial void ratio are selected (0.93 and 0.75) respectively  
96 with the same water content  $w$  (0.15).

97 The soil water retention curve (WRC), obtained using the suction controlled oedometric cell  
98 (Romero et al. 1995), is presented in Figure 2 in terms of suction and saturation degree relationship.  
99 Experimental data refer to the main wetting curve obtained for two different void ratios, 0.93 and  
100 0.75 respectively; both of them has been fitted using Van Genuchten (1980) equation the parameters  
101 of which are reported in Table 3. In the suction range experimentally studied, as porosity decrease air  
102 entry value ( $1/\alpha$ ) increases from 50 to 166 kPa and the slope of the transition ( $n$ ) zone reduces from  
103 1.4 to 1.3 in the  $S_r-s$  plane. The findings are consistent with literature results (Gens *et al.*, 1996;  
104 Romero, 1999; Romero & Vaunat, 2000; Fredlund & Xing, 1994; Tarantino & De Col, 2008, Romero  
105 *et al.* 2011). Neglecting for the sake of simplicity the hysteresis of WRC, the as-compacted suction,  
106 according to Van Genuchten (1980) equation, is respectively 900 kPa and 3400 kPa for  $e_0=0.93$   
107 ( $S_{r0}=0.43$ ), and  $e_0=0.75$  ( $S_{r0}=0.52$ ).

## 108 MODEL AND INSTRUMENTATION

109 For the purpose of the experiment, 180 mm of soil are statically compacted imposing a constant  
110 displacement rate ( $v=1.5$  mm/min), under one-dimensional condition, in a rigid cylindrical container  
111 of 300 mm of diameter. A 10 mm thick sand layer, surrounded by geotextile, is laid as drainage layer  
112 at the bottom of the model. A 2 mm thick plastic sheet is placed at the border to reduce the  
113 container's roughness and shear stresses developing during model preparation. To prevent water  
114 evaporation in the upper part of the model, a plastic film covers the soil surface. The bored pile is  
115 installed at  $1\times g$ , the pre-hole has been realized by means of a manual screwing system of the  
116 IFSTTAR facilities (Khemakhem et al., 2010) for an embedded length of 150 mm.

117 The bottom of the model is connected to a water reservoir the level of which is governed by an  
118 electro-pneumatic valves system directly controlled by the operator in the centrifuge control room.  
119 A laser sensor measures the water height in the tank.

120 The model has been extensively instrumented in order to follow both the equalization phases and  
121 pile loading, a schematic view of the instrumentation used is proposed in Figure 3. Five LVDT  
122 sensors measure soil settlements, two of them are far from the expected interaction zone and they  
123 measure the settlements due to flight and consolidation only, the other three are in line with applied  
124 load, in the passive area, and can measure also the soil movement during pile loading. The pore water  
125 pressure (negative and positive) in the soil is measured with three tensiometers, placed at different  
126 depth at the model border. The sensor's range is -500 kPa to 500 kPa. The sensor calibration and  
127 saturation procedure of the tensiometer and of the porous stone are described by Mancuso (2011).

128 The load has been applied at 35 mm from ground level by a hydraulic actuator. The loading phase  
129 was displacement-controlled ( $v=0.003$  mm/s at model scale), and a load cell (full scale 2500 N)  
130 provided the measure of lateral load. One LVDT built in on a rotational joint gives pile's vertical  
131 displacement and rotation.

132 At the end of each test, undisturbed specimen were sampled all along the model height in order  
133 to obtain water content and void ratio distribution with depth.

#### 134 MODEL PILE CHARACTERISTICS

135 The 1/100 model pile is a close-ended tube, instrumented with 10 pairs of strain gauges arranged  
136 every 15 mm, Figure 4. After a calibration in the lab, the set of gauges deliver the bending moment  
137 profile along the pile length. At the prototype scale ( $N=100\times g$ ) the model represents a full circular  
138 pile of 1.2 m of diameter, 15 m of embedded length with a bending stiffness of  $3.9$  GNm<sup>2</sup>, subjected  
139 to a lateral load applied at 3.5 m from ground surface. The combination of high bending stiffness  
140 and relatively small slenderness ratio ( $L/D = 15/1.2 = 12.5$ ) led to a substantial rigid behaviour of  
141 the pile.

## 142 Centrifuge test and procedures

### 143 MODEL PREPARATION

144 The soil model used in the centrifuge model has been statically compacted in six layer, with the  
145 same procedure followed for the laboratory tests, with  $w=15\%$  and  $e_0=0.93$  or  $0.75$  and it is located  
146 on 'dry side' of the Proctor curve. The distribution of vertical compaction stresses, measured during  
147 compaction and reported in Figure 5, shows a reasonably good homogeneity for any sample and a  
148 very good repeatability of the results in different tests. The compaction stress increases with dry  
149 density from a mean value of 500 kPa in the looser state ( $e_0=0.93$ ) to 1400 kPa in the denser state  
150 ( $e_0=0.75$ ). The homogeneity and repeatability are confirmed also by cone penetration tests (with a  
151  $d_c=12$  mm) at  $1\times g$  reported in Figure 6, referring to low compacted soil. The curves have a similar  
152 trend with an increase with depth up to  $z\sim 50$  mm and then are characterized by a mean constant  
153 value of  $q_c\sim 3.6$  MPa.

### 154 EXPERIMENTAL PROGRAMME

155 The tests performed in centrifuge are nine, four of them are presented in details, focusing the  
156 attention on two parameters: Initial void ratio (2 cases)

- 157 • Elevation of the water table (2 cases)

158 The testing programme is resumed in Table 4 where  $z_w/L$  is the water table elevation to embedded  
159 length ratio and  $e_0$ ,  $w_0$ ,  $\sigma_{vc}$  and  $Sr_0$  are, respectively, the initial void ratio, the gravimetric water content,  
160 the compaction stress and the degree of saturation. These values have to be intended as mean values  
161 of soil properties.

### 162 PROCEDURE

163 In the main tests (T\_06 and T\_08) the pile is loaded in unsaturated conditions, until a normalized  
164 lateral displacement,  $y/D$ , of 30-40% was reached. Then, the water table  $z_w$ , has been imposed at 7 m  
165 (prototype scale) from ground level. The water table elevation over the embedded length ratio is close  
166 to 0.5 ( $z_w/L = 7/15 = 0.46$ ).



167 In the following step, the actuator control has been switched from displacement to force control  
168 and the water table level has been raised quickly to ground level. The instrumentation on the pile  
169 allowed continuous monitoring of head displacement, rotation and bending moments along pile  
170 during water table rising.

171 For the sake of comparison, a pile load has been conducted up to soil failure in fully saturated  
172 condition,  $z_p=0$  (T\_05 and T\_09).

### 173 TEST STEPS

174 The following steps characterize the main tests (T\_06, T\_08):

- 175 1)  $1\times g$  imbibition: a zero pore pressure is applied at the model base in order to reduce after  
176 compaction suction;
- 177 2) Flight and application of hydraulic condition at model base: the system has been left in  
178 equalization for at least 3 hours;
- 179 3) Pile load at displacement control ( $v=0.003$  mm/s);
- 180 4) Increase of water table and equalization.

181 For reference tests in fully saturated condition (T\_05 and T\_09), only the first three steps are  
182 needed; the water table has been directly imposed at ground level.

### 183 Results and discussion

184 In this section are presented selected results to illustrate the influence of soil state condition and  
185 partial saturation on the response of laterally loaded piles. The complete results of the experimental  
186 program are detailed in Lalicata (2018).

187 General consideration about soil state at the end of the reference tests on saturated soil for  $e_0=0.93$   
188 (T\_05) and  $e_0=0.75$  (T\_09) can be deduced by the analysis of the water content and the void ratio  
189 distribution with depth reported in Figure 7. Data shows that for  $e_0=0.93$  (T\_05) void ratio decreases  
190 with depth (typical of soil NC) from a value of  $\sim 0.9$  at surface to a value of 0.76 for a depth of 17 m;  
191 on the other hand, in T\_09 ( $e_0=0.75$ ) the void ratio is mostly constant over the entire range of depth.  
192 Moreover, the comparison of the experimental data with the oedometric normal consolidation line,

193 grey line in Figure 7, highlights how the loose soil lays on the NCL below 4 meters of depth, while  
 194 the denser ones intercept it at 12 meters from ground level. These differences, even for the same  
 195 stress history prior to pile loading ( $1\times g$  imbibition, increase of total stress and in-flight equalization),  
 196 may be ascribed both on the different initial void ratio and the different shape of the WRC that  
 197 controls the variation of mean effective stress and the preconsolidation pressure during hydro-  
 198 mechanical stress paths (Lalicata, 2018).

#### 199 LATERAL LOAD AT CONSTANT WATER TABLE LEVEL

200 The load-displacement curves for samples in fully saturated conditions and different void ratio  
 201 are shown in Figure 8, at the prototype scale. The lateral displacement measurement,  $y$ , refers to the  
 202 displacement at the load application point (nominally 3.5 m above ground level). In the range of  
 203 lateral displacement explored, the load-displacement relationship is highly non-linear (Rosquoët,  
 204 2007; Mayne et al., 1995, Russo, 2016).

205 The experimental data can be adequately fitted by means of a hyperbolic function (Mayne et al.,  
 206 1995):

$$207 \quad H = \frac{y}{\left( \frac{1}{K} + \frac{1}{H_{lim}} y \right)} \quad (1)$$

208 Where  $K$  [MN/m] is the initial stiffness and  $H_{lim}$  [MN] is the asymptotic load. In Figure 8, the  
 209 fitting of hyperbolic function with the load-test data appears to be quite satisfying: dashed and  
 210 continuous lines are used for  $e_0=0.75$  and  $0.93$  respectively. The numerical values of lateral stiffness  
 211 and ultimate load are reported in Table 5.

212 The strength mobilized, under the applied lateral displacement, is different in asymptotic value  
 213 and shape for denser and looser samples: for every  $y$  value, the  $H/H_{lim}$  ratio is higher for  $e_0=0.93$   
 214 compared to  $e_0=0.75$ . At the end of the test ( $y=1.6$ m), for the loose soil ( $e_0=0.93$ , T\_05) the measured  
 215 load of 0.7 MN is about the 80% of ultimate capacity  $H_{lim}$ . On the contrary, the denser soil,  $e_0=0.75$   
 216 (T\_09), is still far from the ultimate capacity showing a value of 3.2 MN for the maximum lateral  
 217 displacement applied ( $y=1.4$  m), giving a load ratio,  $H/H_{lim}$ , of 0.55. Initial lateral stiffness increases

218 more than three times as initial void ratio decreases as well. In addition, for low initial void ratio, the  
219 load increases almost linearly for a significant displacement range, up to 0.2 m, suggesting that a small  
220 amount of yielding occurs in the soil. Furthermore, in the looser state the load-displacement  
221 relationship exhibits a non-linear behaviour from low values of displacement, indicating that the soil  
222 develops significant plastic strain even for very low load level (Russo & Viggiani, 2009). The findings  
223 are consistent with the deduced over-consolidation ratio induced by different initial void ratio already  
224 commented.

225 The influence of partial saturation on the load-displacement behaviour is analysed in Figure 9,  
226 where the load-displacement curves for looser (Figure 9a) and denser (Figure 9b) samples are  
227 reported. In both cases, the partial saturation induces higher stiffness to the soil above the water  
228 table, with more appreciable effects for high void ratio. Moreover, for loose soil in presence of partial  
229 saturation the load-displacement relationship exhibits an initial linear branch, which cannot be found  
230 in saturated condition, consistent with the well-known increment of preconsolidation stress in  
231 unsaturated soils (Gens 2010).

232 It is known that stiffness in fine graded saturated soil depends on mean effective stress  $p'$ , void  
233 ratio  $e$  and/or OCR in a non-linear way (Viggiani & Atkinson, 1995; Rampello et al., 1994). Most  
234 recently other researchers have proposed a modified formulation to take into account the effect of  
235 saturation degree and suction on the small strain stiffness (Biglari et al., 2011), in which stiffness  
236 variations are mainly attributed both to the increase of mean effective stress  $p'$  and to increase the  
237 yielding pressure induced by partial saturation (Jommi, 2000; Laloui & Nuth, 2009; Tamagnini, 2004).

238 Following the generalized effective stress framework (Laloui & Nuth, 2009; Bishop & Blight,  
239 1963), in unsaturated conditions the main effective stress increases ( $T_{06}$  and  $T_{08}$ ), compared to  
240 saturated ones ( $T_{05}$  and  $T_{09}$ ), of the quantity  $\Delta p' = \gamma_w \cdot z \cdot (S_r - 1) - \gamma_w \cdot z_w \cdot S_r$ . On the other hand,  
241 as expected, the stiffness increment due to capillary forces, is better appreciated on the loose soil  
242 ( $e_0=0.93$ ,  $T_{06}$ ) which starts from lower values of stiffness. Those increments become less important  
243 as the initial structure increases due to the decreasing of initial void ratio.

244 In addition, the different distribution of saturation degree with depth for the two materials,  
 245 illustrated in Figure 10, plays an important role in the understanding of the observed behaviour. For  
 246 sake of simplicity, the plots are evaluated supposing that pore pressures were in hydrostatic conditions  
 247 ( $u = \gamma_w \cdot z_w$ ); the values of degree of saturation deduced from the SWRC, Table 3, are very different.  
 248 At ground level, where the differences are more pronounced, the reduction of  $S_r$  compared to  
 249 saturated conditions for the looser soils are 4 times higher than that corresponding to the denser soil.  
 250 This difference in the distribution of  $S_r$ , give an increases in the ratio  $p'_{\text{cunsat}}/p'_{\text{csat}}$  between the  
 251 preconsolidation pressure in unsaturated conditions  $p'_{\text{cunsat}}$  and in saturated conditions  $p'_{\text{csat}}$ , which is  
 252 properly described with a exponential function of the degree of saturation (e.g. Jommi 2000;  
 253 Tamagnini 2004; Gallipoli et al 2003). As well as the stiffness and the strength increase with the  
 254 decreasing of  $S_r$ .

255 Table 5 summarizes the relative influence of the position of water table,  $z_w/L$ , and soil state for  
 256 lateral stiffness  $K$  and ultimate load  $H_{lim}$  respectively, evaluated by means of eq. (1). Passing from  
 257  $z_w/L = 0$  to  $z_w/L = 0.46$  it can be observed a stiffness increment of more than 300% for high initial  
 258 void ratio and of 50% low initial void ratio. Therefore, structure effects induced by partial saturation  
 259 are significantly important for soil with initial open structure because of lower values of saturation  
 260 degree which allows developing higher bonding effect induced by meniscus. A direct connection  
 261 between lateral stiffness  $K$  and soil stiffness  $E_s$  cannot be easily recognised because of the pile behaves  
 262 almost like a rigid pile, hence the head displacement is the sum of a deflection and a rigid rotation  
 263 (Lalicata, 2018) and elastic solutions (Randolph 1981, Higgins et al. 2013, Di Laora and Rovithis  
 264 2015) are not directly applicable. In comparison with lateral stiffness,  $H_{lim}$  appears to be less affected  
 265 by partial saturation: compared to saturated condition, gains are 12% for  $e_0 = 0.75$  and 220% for  $e_0 =$   
 266 0.93.

267 The comparison of bending moment profiles, at 0.1 MN of applied load, for T\_08 and T\_09 ( $e_0$   
 268 = 0.75) is presented in Figure 11 (a). The pile does not behaves as a purely flexible pile, since bending  
 269 moment propagates all along the entire embedded length then the active length of the pile is equal,  
 270 or even greater of, to the actual length  $L$  (Randolph, 1981). The stiffness increment in the shallower

271 seven meters from ground level, induced by partial saturation, led to a reduction of maximum bending  
272 moment of more than 20% for  $H=0.1$  MN. Thanks to partial saturation, the position of maximum  
273 bending moment slightly moves upward passing from 5 to 4 meter from mudline. The small  
274 differences of the moment measured at the ground level in the two cases may be ascribed to the  
275 different settlement of the soil during the consolidation phase (Lalicata, 2018).

276 Double derivation of moment profile allows calculating the soil pressure distribution along the  
277 pile for every load increment. Soil pressure distribution is shown in Figure 11 (b) for the same soil  
278 condition and load level of Figure 11 (a). In the shallower part, the unsaturated soil hold higher  
279 pressure compared to the saturated one. Pressure remains almost constant in the first 6 meters from  
280 ground level and then it reduces smoothly towards the pile tips changing sign at 12 meter of depth.

281 Referring to almost rigid piles, the findings reported in the present study seems to indicate that  
282 the unsaturated zone above water table can change significantly the soil reactions distribution all  
283 along the pile length.

284 The ratio of maximum bending moment obtained for unsaturated condition and saturated  
285 condition remains at the constant value of 0.76 for relatively low lateral load, up to 0.5 MN, then it  
286 gradually increases to 0.94 measured for  $H=2.1$  MN, as with the increase of the applied load the rigid  
287 behaviour becomes dominant compared to the flexural one in both cases (Figure 12).

288 The bending moment profiles of T\_06 and T\_08, relative to 0.1 MN of lateral load, are pointed  
289 out in Figure 13. This comparison allows to highlight the influence of soil stiffness, here mainly  
290 related to initial void ratio and different  $S_v$  distribution, on bending response of the pile: as for softer  
291 soil (T\_06,  $e_0 = 0.93$ ) the interaction involves greater volumes of soil compared to stiffer ones (T\_08,  
292  $e_0 = 0.75$ ). As expected, the bending moment increases as soil stiffness decreases, and as for the looser  
293 sample (T\_06), the bending moment distribution is more homogeneous along the entire pile length  
294 and the maximum bending moment takes place at greater depth. It is worth noting that all these  
295 results are significantly affected by the moment at ground level induced by load eccentricity that  
296 significantly increases the values of the maximum bending moment and the downward load transfer  
297 (Budhu & Davies, 1987).

298

## WATER TABLE RISING AT CONSTANT LOAD

299 For T\_06 and T\_08, when the lateral head displacement has reached the 30-40% of the diameter,  
300 the loading phase has been stopped and the actuator has been switched from displacement control  
301 to loading control. By the electro-pneumatic valves system, the pore pressure at the bottom of the  
302 model has been raised quickly from 120 kPa to 190 kPa, in order to simulate the water table raising  
303 from 7 m of depth to 0 m. The model has been left in equalization for the remaining time test (320  
304 min for T\_06 and 380 min for T\_08, at model scale), the analysis of soil settlements and pore pressure  
305 evolution indicates that the stationary condition has not been reached in none of the tests (Lalicata,  
306 2018).

307 Suction decreases, due to imbibition, led to a reduction of mean effective stress and of the  
308 preconsolidation pressure (where the collapse for saturation occurs), as well as of the soil stiffness  
309 and strength. As a result, the pile head displacement has increased in both tests (Figure 14).  
310 Displacement increment resulted higher for open soil structure, T\_06, than for closer one, T\_08. The  
311 global response reported in Figure 14 (a) and (b) is the result of a combination of multiple factors  
312 such as differences in saturated permeability, different soil stiffness prior to loading and load ratio  
313 level between initial load and ultimate load in saturated condition. First, since saturated permeability  
314 decreases with void ratio and, in this phase, the hydraulic equilibrium was far to be reached, lower  
315 values of pile lateral displacement are expected for the model with  $e_0=0.75$ . Secondly, for the same  
316 perturbation applied, higher displacement is expected for loose soil ( $e_0=0.93$ ) because of lower  
317 stiffness. Finally, looking at the comparison between the load-displacement relationship for saturated  
318 and unsaturated condition, it seems reasonable to suppose that for  $e_0=0.93$  (Figure 14 (a)) a lateral  
319 load of 1.2 MN it is not sustainable in fully saturated conditions; while, for  $e_0=0.75$  even with no  
320 suction (Figure 14 (b)), a value of 2.1 MN appears to be sustainable by soil, then the system could  
321 have advanced faster to collapse in the first case. However, it is to be noted that the load-deflection  
322 curve obtained in saturated conditions (i.e. T\_09) not necessarily represents a lower bound solution,  
323 given that soil behaviour is strongly nonlinear and dissipative, therefore the final point measured  
324 during saturation (grey triangles in Figure 14 (b)) did not represent the end of the process.

325 The evolution of head displacement with the centrifuge time and the pore pressure for the two  
326 tests are presented in Figure 15 (a) and (b). In both Figures, black line refers to  $e_0=0.93$  (T\_06), grey  
327 colour is used for  $e_0=0.75$  (T\_08); in Figure 15 (b) different tensiometers position with depth is  
328 illustrated with various style line: a continuous line has been used for  $z=4\text{m}$ , large dashes for  $z=9\text{m}$   
329 and, finally, small dashes has been used for  $z=14\text{m}$ . In order to better emphasize the phenomena, the  
330 results are represented in a semi-logarithmic plane and time has been replaced to zero just before the  
331 increase of water pressure. Instead of elapsed time, the Terzaghi non-dimensional formulation for  
332 time factor has been used:  $T = \frac{c_v}{H^2}t$ , where  $c_v$  is the coefficient of vertical consolidation,  $t$  is the  
333 elapsed time and  $H$  is the drainage layer. For sake of simplicity the same reference values of  $c_v$  and  $H$   
334 are adopted for all the tests and are  $1.0 \times 10^{-6} \text{ m}^2/\text{s}$  (Table 2) and 180 mm (initial soil model height)  
335 respectively. It is interesting to note that, even if no stabilization occurs, the slope of the pore pressure  
336 curves gradually reduces, while the increment of lateral displacement keeps growing; moreover, in  
337 the last part of the test, a slight increment of displacement rate can be observed for T\_06.

338 During saturation, the strength reduction in upper part produced the reduction of soil pressure  
339 against the pile in the first meters of depth from ground level and an increase in the last meters.  
340 Observing the bending moment profiles prior and post water table rising, it can be observed (Figure  
341 16) a general increment of the moment below the position of the maximum bending moment (from  
342 6 m to 15 m of depth). Since the pile undergoes a rigid body motion during saturation the maximum  
343 bending moment variation is less than 10%.

## 344 **Conclusion**

345 In the present work, the soil pile interaction under lateral loading in unsaturated condition, by  
346 means of centrifuge tests has been studied. The models have been statically compacted at two  
347 different void ratios and the same water content. The initial conditions have been chosen based on a  
348 wide set of flooding tests at different void ratios and water content with the aims to cover a range of  
349 void ratios representative of *in situ* soil conditions.

350 The pile has been loaded with two positions of water table: one at half of pile's embedded length  
351 ( $z_w = 7$  m) and the other at ground level ( $z_w = 0$  m). Compared to saturated conditions, a significant  
352 increase in lateral stiffness on the load-deflection relationship: 300% for loose soil ( $e_0=0.93$ ) and 50%  
353 for dense soil ( $e_0=0.75$ ) has been observed in both cases. The effect of partial saturation is stronger  
354 for the looser state as, for the same suction, bonding effects due to capillary forces gives a major  
355 increment in soil structure. Moreover, the major changes of  $S_r$  in the looser sample is given to the  
356 different shape of WRC with void ratio.

357 The present study focus on the behaviour of an almost rigid pile and additional tests are required  
358 to investigate the effect of partial saturation varying the soil-pile relative stiffness and the slenderness  
359 ratio. In the particular case of rigid pile, that involves a significant volume proportional to the entire  
360 embedded length, the increase of soil stiffness in the shallower soil layer leads to a reduction of  
361 maximum bending moment more than 20% that moves towards ground surface. For flexible piles  
362 that have a critical length lower than the embedded length, the pile response is strongly dependent  
363 from the stiffness of the soil close to the surface. Therefore, it is possible that stiffness variation  
364 induced by partial saturation may will have more visible effects for flexible piles compared to the  
365 rigid pile of this study, which represents a lower bound solution in the understanding of the role of  
366 partial saturation in horizontally loaded piles

367 During saturation, due to the combination of excessive load level and strong variation of water  
368 table level, the system goes towards soil collapse with a close to rigid body motion. Findings appear  
369 to show that neglecting the presence of partial saturation is not necessarily a safety solution when  
370 significant variation of saturation degree takes place. Reduction of soil strength and stiffness due to  
371 saturation can lead to greater pile head displacement than those predicted by fully saturated analysis.  
372 The increase of lateral displacement depends both on of the value of the load and the initial water  
373 table position.

#### 374 **Acknowledgments**

375 This research has been performed in the framework of the GEO-TRANSALP-PILE-UNSAT  
376 agreement developed between DISG, the "Department of Structural and Geotechnical Engineering"



377 of "Sapienza" University of Rome, "Department of Department of Civil and Computer Engineering"  
378 University of Rome "Tor Vergata" and IFSTTAR, the "French Institute of Science and Technology  
379 for Transport, Development and Networks". They are greatly acknowledged. The authors would like  
380 to thank the technical team of the Ifsttar's geo-centrifuge, the technical staff of DISG geotechnical  
381 laboratory and also Dr. M. Blanc for his advices.

## 382 **References**

383 Banerjee P.K., Davies T.G. (1978). The behaviour of axially and laterally loaded single piles  
384 embedded in nonhomogeneous soils. *Géotechnique*, 28 (3), 309 – 326.

385 Biglari, M., Mancuso, C., d'Onofrio, A., Jafari, M. K., Shafiee, A. Modelling the initial shear  
386 stiffness of unsaturated soils as a function of the coupled effects of the void ratio and the degree of  
387 saturation. *Computers and Geotechnics*, 38 (2011) 709–720.

388 Bishop, A., Blight, G., (1963). Some aspects of effective stress in saturated and partly saturated  
389 soils. *Géotechnique* 13, 177–197.

390 Budhu M., Davies T.G. (1987). Nonlinear analysis of laterally loaded piles in cohesionless soils.  
391 *Can. Geotech. J.*, 24 (2), 289 – 296.

392 Caicedo, B., Medina, C., Cacique, A. (2006). Validation of time scale factor of expansive soils in  
393 centrifuge modeling. *Physical modeling in Geotechnics ICPMG06*, Ng, Zhang, Wang (eds), 273–277.

394 Caicedo, B., Thorel, L. (2014). Centrifuge Modelling of Unsaturated soils. *Special Issue « Advances  
395 in the Mechanics of Unsaturated soils » of the Journal of Geoengineering Sciences*. Vol.2,n°1-2, 83-103 (july 2014)  
396 DOI 10.3233/JGS-130013.

397 Casini, F., (2008). Effetti del grado di saturazione sul comportamento meccanico di un limo. *Ph.D.  
398 thesis*, Università degli studi di Roma La Sapienza.

399 Casini, F., Vaunat, J., Romero, E., Desideri, A., (2012). Consequences on water retention  
400 properties of double-porosity features in a compacted silt. *Acta Geotechnica* (2012) 7:139–150.

401 Corté J.F. (1989) Model testing-Geotechnical model tests, *Proc. XII ICSMFE Rio*, 2553-2571.

402 Cui, Y., Delage, P., (1996). Yielding and plastic behaviour of an unsaturated compacted silt.  
403 *Géotechnique*, 46 (2), 291–311.

404 Depountis N, Davies MCR, Harris C, Burkhart S, Thorel L, Rezzoug A, Konig D, Merrifield C,  
405 Craig WH. Centrifuge modelling of capillary rise, *Engineering Geology*, 2001;60(1-4):95-106. ISSN:  
406 0013-7952 .

407 Di Laora, R., Rovithis, E. (2015). Kinematic Bending of Fixed-Head Piles in Nonhomogeneous  
408 Soil. *J. Geotech. and Geoviron. Eng.* No141.

409 Escario, V., Saez, J., (1986). The shear strength of partly saturated soils. *Géotechnique*, 36 (3), 453–  
410 456.

- 411 Fredlund, D.G., Xing A., (1994). Equation for the soil-water characteristic curve. *Can. Geotech. J.*  
412 31 (4), 521–532.
- 413 Gens, A., (2010). Soil–environment interactions in geotechnical engineering. *Géotechnique*, 60 (1),  
414 3–64.
- 415 Gens, A., Alonso, E. E., Surlol, J., Lloret, A. (1996). Effect of structure on the volumetric  
416 behaviour of a compacted soil. *Proc. 3<sup>rd</sup> Int. Conf.on Unsaturated Soils, Paris 1*, 83-88.
- 417 Georgiadis K., Potts D.M. & Zradkovic L. (2003). The influence of partial saturation on pile  
418 behavior. *Géotechnique*, 53 (1), 11 – 25.
- 419 Higgins, W., Vasquez, C., Basu, D., Griffiths, D.V. (2013). Elastic solution for laterally loaded  
420 piles. *Journal of Geotechnical and Geoenvironmental Engineering*. No 139, 1096-1103.
- 421 Jommi, C. (2000). Remarks on the constitutive modelling of unsaturated soils. *Proc. Experimental*  
422 *Evidence and theoretical Approaches in Unsaturated Soils*, Tarantino & Mancuso (eds), Balkema, Rotterdam,  
423 139-153.
- 424 Khemakhem, M., Chenaf, N., Garnier, J., Rault, G., Thorel, L., Dano, C. Static and cyclic lateral  
425 pile behavior in clay. *7th International Conference on Physical Modelling in Geotechnics 2010*, ICPMG  
426 2010Volume 2, 2010, Pages 953-958.
- 427 Krishnan R., Gazetas G., Velez A. (1983). Static and dynamic lateral deflexion of piles in non –  
428 homogeneous soil stratum. *Géotechnique*, 33 (3), 307 – 325.
- 429 Lalicata, L. 2018. Effect of saturation degree on the mechanical behaviour of a single pile  
430 subjected to lateral forces (in Italian). *Ph.D Thesis*, Sapienza Università di Roma.
- 431 Laloui, L., Nuth, M. (2009). On the use of the generalised effective stress in the constitutive  
432 modelling of unsaturated soils. *Comp and Geotech.* 36, 20-23.
- 433 Mancuso, C. et al. (2011) . Messa a punto di un nuovo minitensiometro ad alta capacità. *LARG*.
- 434 Mayne, P.W., Kulhawy, F. H., Trautmann, C. H., (1995). Laboratory Modeling of Laterally-  
435 Loaded Drilled Shafts in Clay. *J. Geotech. Eng.*, 1995, 121(12): 827-835.
- 436 Rampello, S., Silvestri, F. & Viggiani G. (1994b). The dependence of  $G_0$  on stress state and history  
437 in cohesive soils. *Proc. 1st Int. Conf. Pre-failure Deform. Character. Geomater.*, Sapporo 2, 1155-1160.
- 438 Randolph M.F. (1981). The response of flexible piles to lateral loading. *Géotechnique*, 31 (2), 247 –  
439 259.
- 440 Romero, E., (1999). Characterization and thermo-hydro-mechanical behaviour of unsaturated  
441 Boom clay: an experimental study. *Ph.D. thesis*. Universitat Politècnica de Catalunya Barcelona, Spain.
- 442 Romero, E., Della Vecchia, G., Jommi, C. (2011). An insight into the water retention properties  
443 of compacted clayey soils. *Géotechnique* 61, (4), 313–328.
- 444 Romero, E., Lloret, A., Gens, A., (1995). Development of a new suction temperature controlled  
445 oedometer cell. In: Alonso, E., Delage, P. (Eds.), *1st Int. Conf. on Unsaturated Soils*, Paris. Balkema.

- 446 Romero, E., Vaunat, J., (2000). *Retention curves of deformable clays*. Proc. Experimental Evidence and  
 447 theoretical Approaches in Unsaturated Soils, Tarantino & Mancuso (eds), Balkema, Rotterdam, 90-  
 448 106.
- 449 Rosquoët, F., Thorel, L., Garnier, J., Canepa, Y. 2007. Lateral cyclic loading of sand-installed piles.  
 450 *Soils and Foundations* 47(5), 821-832.
- 451 Russo, G. (2016). A method to compute the non-linear behavior of piles under horizontal loading.  
 452 *Soils and Foundation*. 56 (1), 33-43.
- 453 Russo, G., Viggiani, C. (2009). Piles under horizontal load: an overview. *Proceedings of the Second*  
 454 *BGA International Conference on Foundations*, ICOF2008. Brown M. J., Bransby M. F., Brennan A. J. and  
 455 Knappett J. A. (Editors).
- 456 Salager, S., Nuth, M., Ferrari, A., Laloui, L., (20013). Investigation into water retention behaviour  
 457 of deformable soils. *Can. Geotech. J.* (50), 200–208.
- 458 Schofield, A. N. (1980). Cambridge geotechnical centrifuge operation. *Geotechnique* 30, No. 1, 229–  
 459 267, <http://dx.doi.org/10.1680/geot.1980.30.3.227>
- 460 Sivakumar, V., Wheeler, S. J., (2000). Influence of compaction procedure on the mechanical  
 461 behavior of an unsaturated compacted clay Part 1: Wetting and isotropic compression. *Geotechnique*,  
 462 50 (4), 359–568.
- 463 Soranzo, E., Tamagnini, R., and Wu, W. 2015. Face stability of shallow tunnels in partially  
 464 saturated soil: centrifuge testing and numerical analysis. *Géotechnique*, 65(6): 454–467.
- 465 Tamagnini, R., (2004). An extended cam-clay model for unsaturated soils with hydraulic  
 466 hysteresis. *Géotechnique* 54, 223–228.
- 467 Tarantino, A. & De Col, E. (2008). Compaction behaviour of clay. *Géotechnique* 58, No. 3, 199–  
 468 213.
- 469 Thorel, L. et al. (2011). Physical modelling of wetting-induced collapse in embankment base.  
 470 *Geotechnique* 61 (5), 409–420.
- 471 Van Genuchten, M. T., 1980. A closed-form equation for predicting the hydraulic conductivity of  
 472 unsaturated soils. *Soil Sci. Soc. Am.* 44 (1), 892–898.
- 473 Vanapalli, S.K. (2009). Shear strength of unsaturated soils and its applications in geotechnical  
 474 engineering practice. *Keynote lecture, Proc., 4th Asia-Pacific Conference on Unsaturated Soils*, Newcastle, 579-  
 475 598.
- 476 Vassallo, R., Mancuso, C., Vinale, F., (2007). Effects of net stresses and suction history on the  
 477 small strain stiffness of a compacted clayey silt. *Can. Geotech. J.* 44 (4), 447–462.
- 478 Viggiani, G. & Atkinson, J. H., (1995). Stiffness of fine-graded soils at very small strains.  
 479 *Géotechnique* 45, (2), 249-265.
- 480 Wheeler, S. J., Sivakumar, V., (1995). An elasto–plastic critical state framework for unsaturated  
 481 soil. *Geotechnique*, 45 (1), 35–53.



**Table 1: Scaling laws for centrifuge modelling.**

Parameter	Scaling law model/prototype
Length	$1/N$
Density	1
Unit weight	N
Stress	1
Strain	1
Force	$1/N^2$
Bending moment	$1/N^3$
Seepage velocity	$1/N$
Consolidation time	$1/N^2$
Capillary rise	$1/N$

483

**Table 2: Index properties and hydro-mechanical properties of B-Grade kaolin.**

w <sub>L</sub> (%)	w <sub>P</sub> (%)	IP (%)	ρ <sub>s</sub> (gr/cm <sup>3</sup> )	C <sub>C</sub> (-)	C <sub>S</sub> (-)	N <sub>0</sub> (-)	φ' (°)	k <sub>sat</sub> (m/s)	c <sub>v</sub> (m <sup>2</sup> /s)
42.2	28.2	14.0	2.66	0.26	0.078	1.36	22	4.0·10 <sup>-9</sup>	1.0·10 <sup>-6</sup>

484

**Table 3: Van Genuchten parameters for different void ratio.**

$e_0$	$S_{r_{sat}}$	$S_{r_{res}}$	$\alpha$	$n$	$m$
(-)	(-)	(-)	(1/kPa)	(-)	(1-1/n)
0.93	1.0	0.16	0.02	1.4	0.2501
0.75	1.0	0.16	0.006	1.3	0.2307

485

**Table 4: Testing programme.**

Name	$e_0$ (-)	$z_w/L$ (-)	$w_0$ (%)	$\sigma_v$ (kPa)	$Sr_0$ (%)
Test 05 T_05	0.93	0.0	15.03	580	42.02
Test 06 T_06	0.93	0.46	14.67	559	41.01
Test 08 T_08	0.75	0.46	14.72	1395	51.03
Test 09 T_09	0.75	0.0	14.72	1395	51.03

486



**Table 5: Lateral stiffness and asymptotic load.**

Test	$z_w/L$ (-)	K (MN/m)	$H_{lim}$ (MN)	$e_0$ (-)
T_05	0.0	1.5	0.9	0.93
T_06	0.46	6.2	2.9	0.93
T_09	0.0	5.0	5.6	0.75
T_08	0.46	7.4	6.3	0.75

487

$C_c$	(-)	slope of normalconsolidation line (NCL) in 1D
$C_s$	(-)	slope of unloading-reloading line (NCL) in 1D
$c_v$	(m <sup>2</sup> /s)	coefficient of vertical consolidation
$D$	(m)	pile diameter
$e$	(m)	eccentricity of lateral load
$e, e_0, e_{opt}$	(-)	void ratio, initial void ratio, optimum void ratio
$E_s$	(MPa)	soil stiffness
$g$	(m/s <sup>2</sup> )	gravitational acceleration
$H, H_{lim}$	(MN)	lateral load, asymptotic lateral load
$IP$	(%)	plastic index
$K$	(MN/m)	initial lateral stiffness
$k_{sat}$	(m/s)	saturated permeability
$L$	(m)	embedded pile length
$m$	(-)	Van Genuchten parameter
$M, M_{sat}$	(MNm)	bending moment, maximum bending moment in saturated condition
$N$	(-)	scaling factor
$n$	(-)	Van Genuchten parameter
$N_0$	(-)	reference void ratio on the NCL_1D at $\sigma'_v=1$ kPa
$OCR$	(-)	over consolidation ratio
$p'$	(kPa)	mean effective stress
$q_c$	(MPa)	cone resistance of CPT test
$s$	(kPa)	matrix suction
$S_r, S_{r0}$	(-)	saturation degree, initial saturation degree
$S_{r_{sat}}, S_{r_{res}}$		saturated saturation degree, residual saturation degree
$u_w$	(kPa)	pore water pressure
$v$	(mm/s)	compaction rate
$v$	(mm/s)	lateral displacement rate
$w, w_0, w_{opt}$	(-)	gravimetric water content, initial gravimetric water content, optimum gravimetric water content
$w_L$	(%)	liquid limit
$w_L$	(%)	plastic limit
$y$	(m)	lateral displacement at the application point
$z$	(m)	depth
$z_w$	(m)	water table position
$\alpha$	(1/kPa)	Van Genuchten parameter
$\gamma_{d,opt}$	(kg/cm <sup>3</sup> )	optimum dry density
$\gamma_s$	(kN/m <sup>3</sup> )	unit weight of solids
$\gamma_w$	(kN/m <sup>3</sup> )	unit weight of water
$\varphi'$	(°)	friction angle

490 **Figure 1: Flooding test results in the compaction plane.**

491 **Figure 2: Main wetting Soil Water Retention curves for B-grade Kaolin.**

492 **Figure 3: Experimental set-up and instrumentation.**

493 **Figure 4: Model pile instrumented with 10 pairs of strain gauges.**

494 **Figure 5: Vertical compaction stress with depth for different models.**

495 **Figure 6: CPT profiles for  $e_0=0.93$ .**

496 **Figure 7: Water content and void ratio with depth after test T\_05 and T\_09.**

497 **Figure 8: Effect of soil state condition on Lateral Load-Displacement curves (prototype scale).**

498 **Figure 9: Load-displacement curves for (a) loose soil ( $e_0=0.93$ ); (b) dense soil ( $e_0=0.75$ ).**

499 **Figure 10: Different distribution of saturation degree due to different porosity.**

500 **Figure 11: Comparison of bending moment distribution along pile for highly compacted soil for  $z_w/L=0$  (T\_09) and  $z_w/L$**   
501  **$=0.46$  (T\_08).**

502 **Figure 12: Maximum bending moment ratio, in unsaturated and saturation condition, for highly compacted soil,  $e_0=0.75$ .**

503 **Figure 13: Comparison of bending moment distribution along pile for  $z_w/L=0.46$  and different initial void ratio.**

504 **Figure 14: Load-displacement curves during saturation for (a) loose soil ( $e_0=0.93$ ); (b) dense soil ( $e_0=0.75$ ).**

505 **Figure 15: Evolution with time during rising table of tests T\_06 and T\_08: a) lateral displacement; b) pore pressure at different**  
506 **depth.**

507 **Figure 16: Bending moment profiles after and before saturation for a)  $e_0=0.93$ ; b)  $e_0=0.75$ .**

508

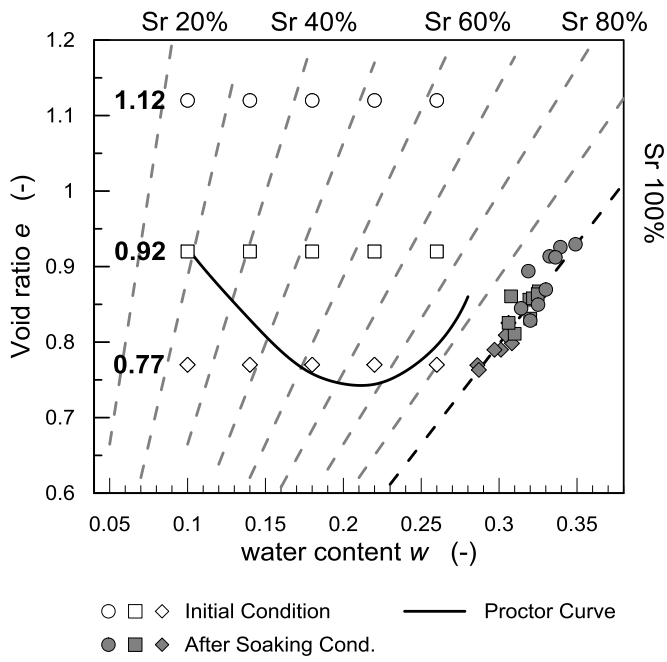


Figure 1: Flooding test results in the compaction plane.

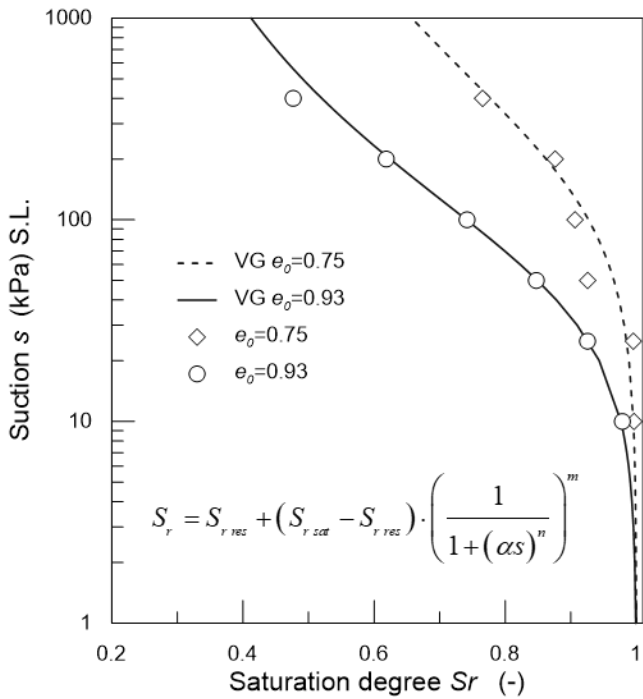


Figure 2: Main wetting Soil Water Retention curves for B-grade Kaolin.

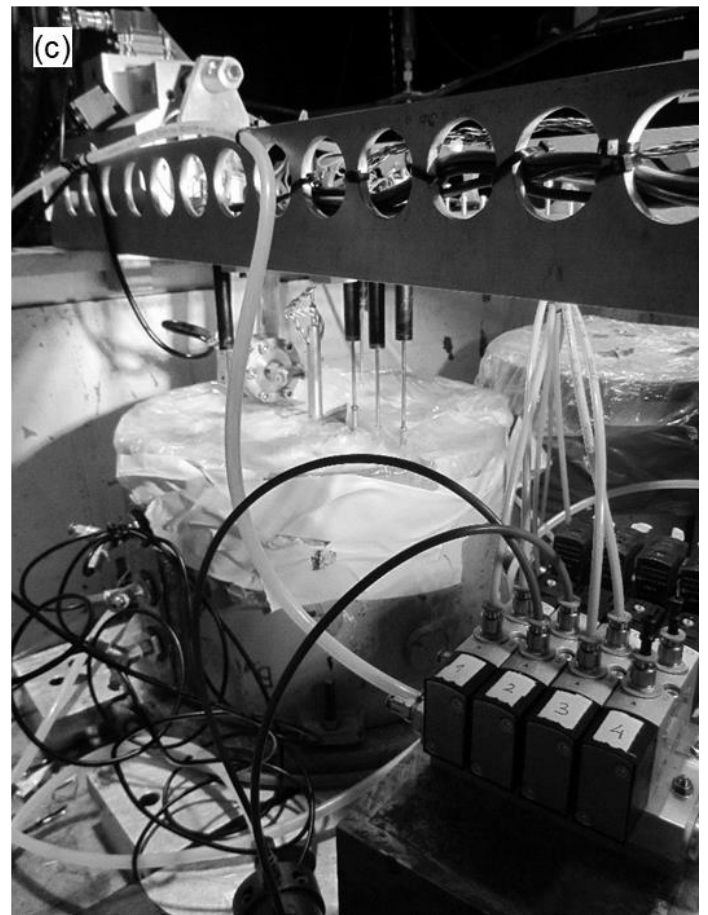
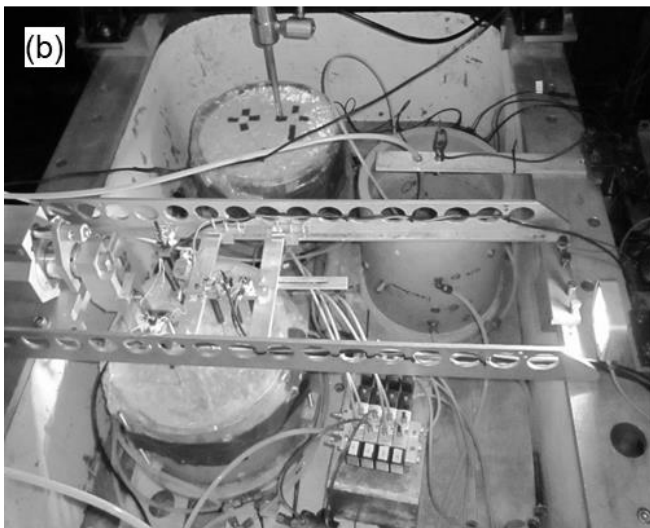
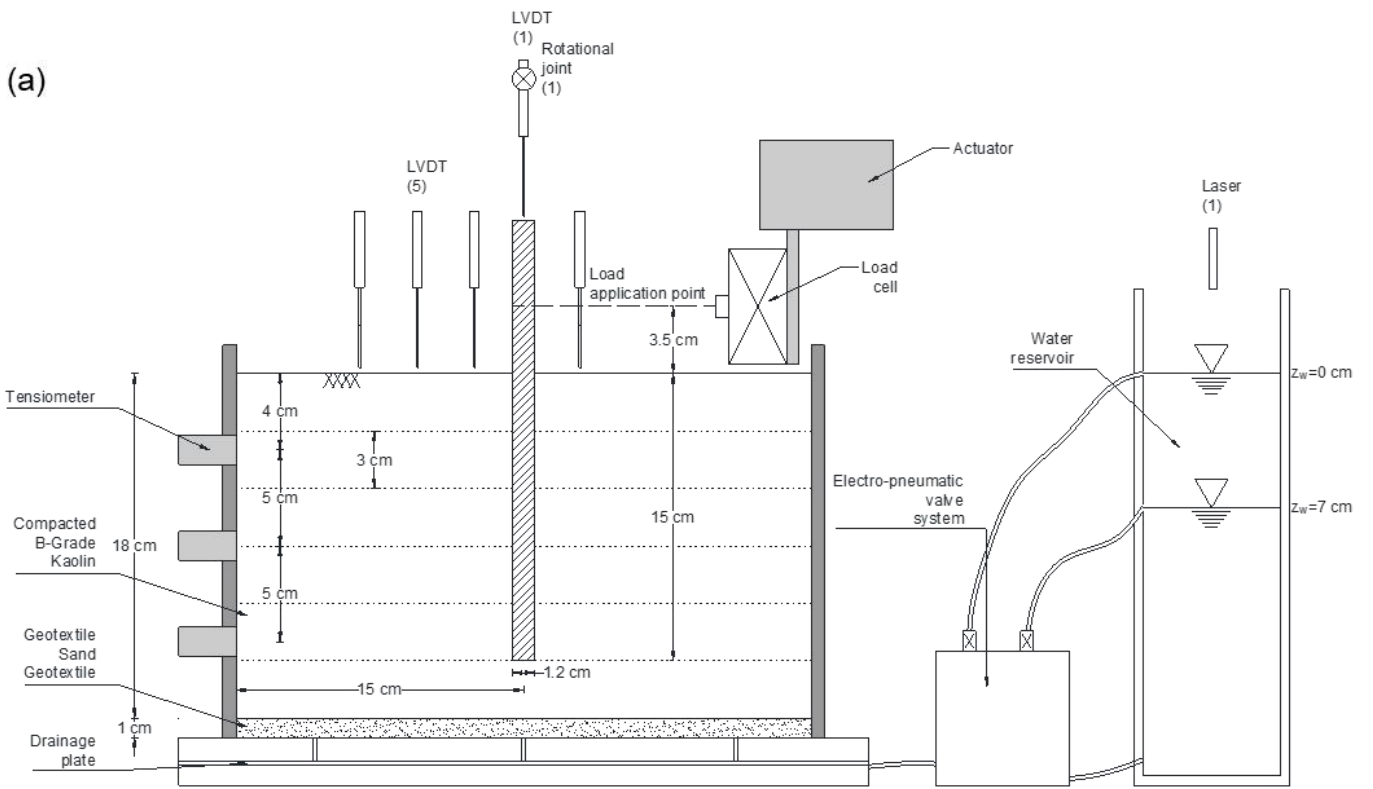


Figure 3: Experimental model: (a) cross section in the load plane, (b) aerial view of the basket, (c) perspective of valve system and soil container, (d) detail of the loading system and LVDT.

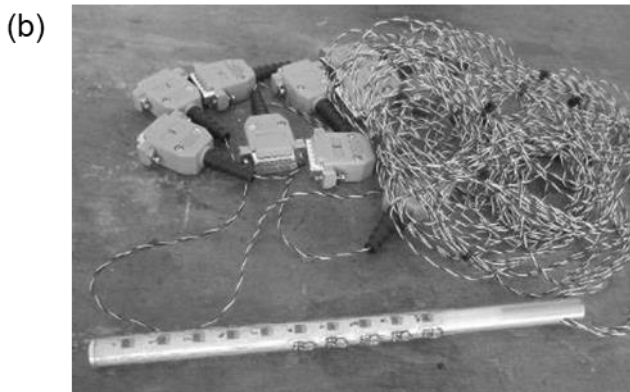
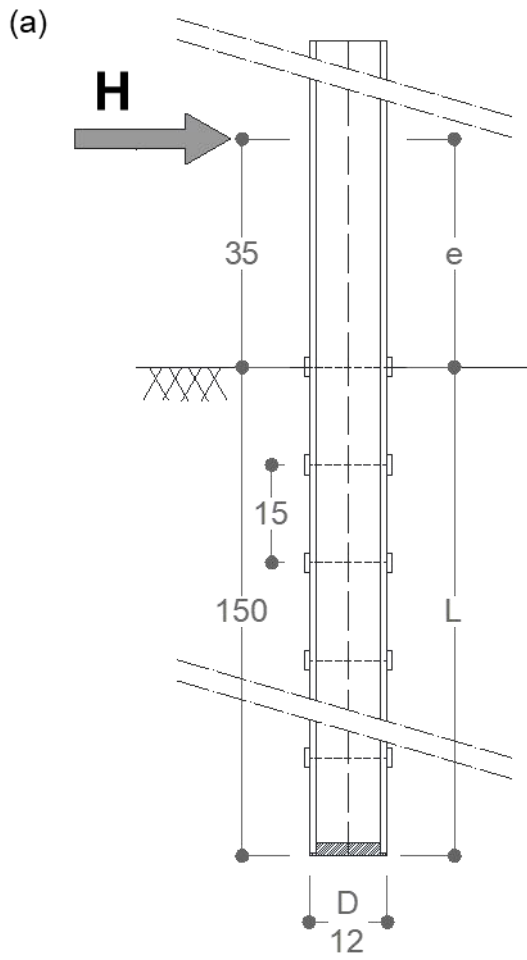
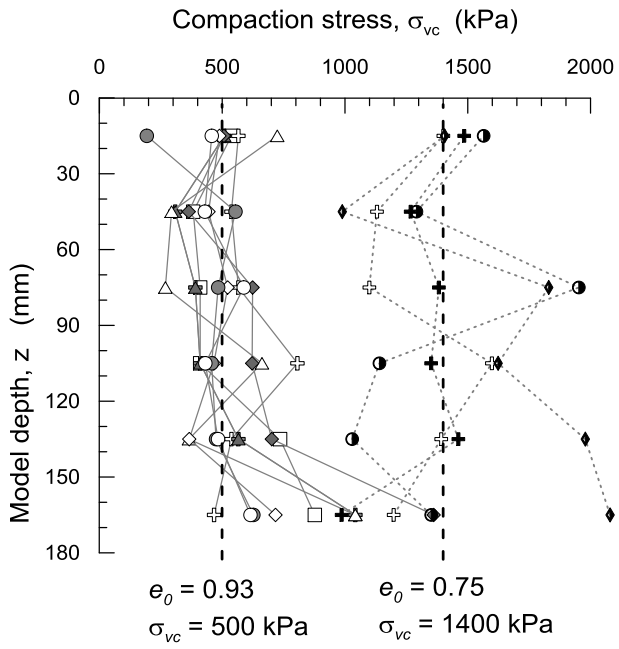


Figure 4: Instrumented model pile: (a) schematic cross section, (b) general view.

518

519

520

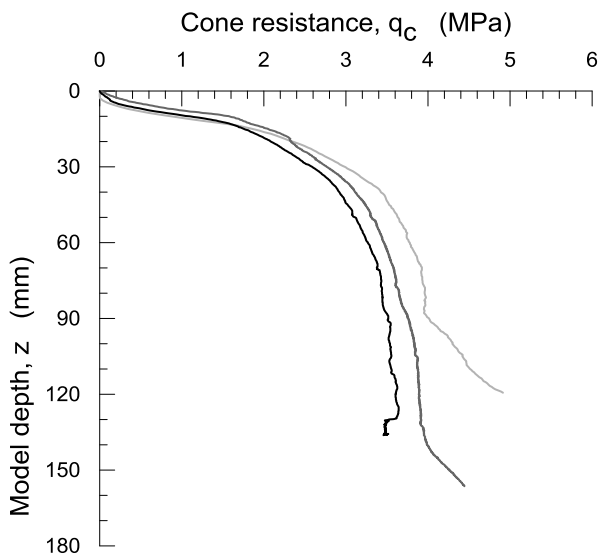


521

522

Figure 5: Vertical compaction stress with depth for different models, each point is located in the middle of one layer.

523



524

525

Figure 6: CPT profiles for  $e_0=0.93$ .

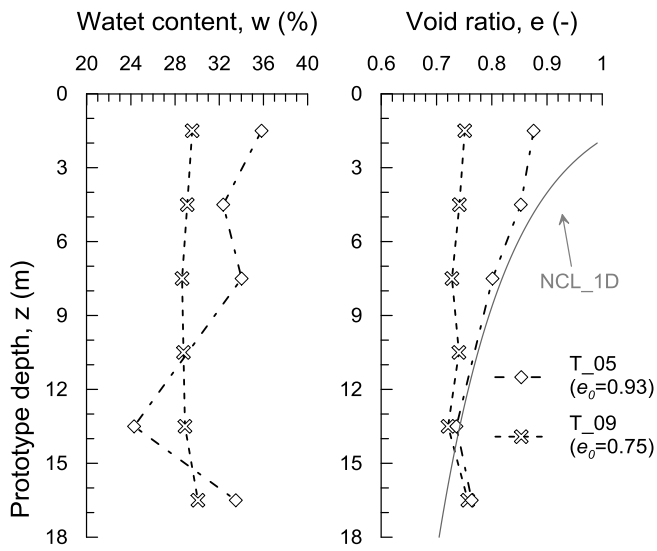


Figure 7: Mean values of water content and void ratio with depth after tests T\_05 ( $e_0=0.93$ ) and T\_09 ( $e_0=0.75$ ).

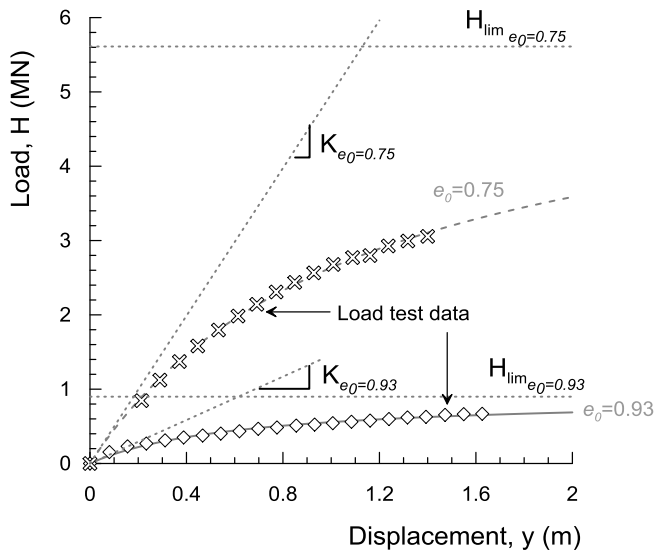


Figure 8: Effect of soil state condition on Lateral Load-Displacement curves (prototype scale).



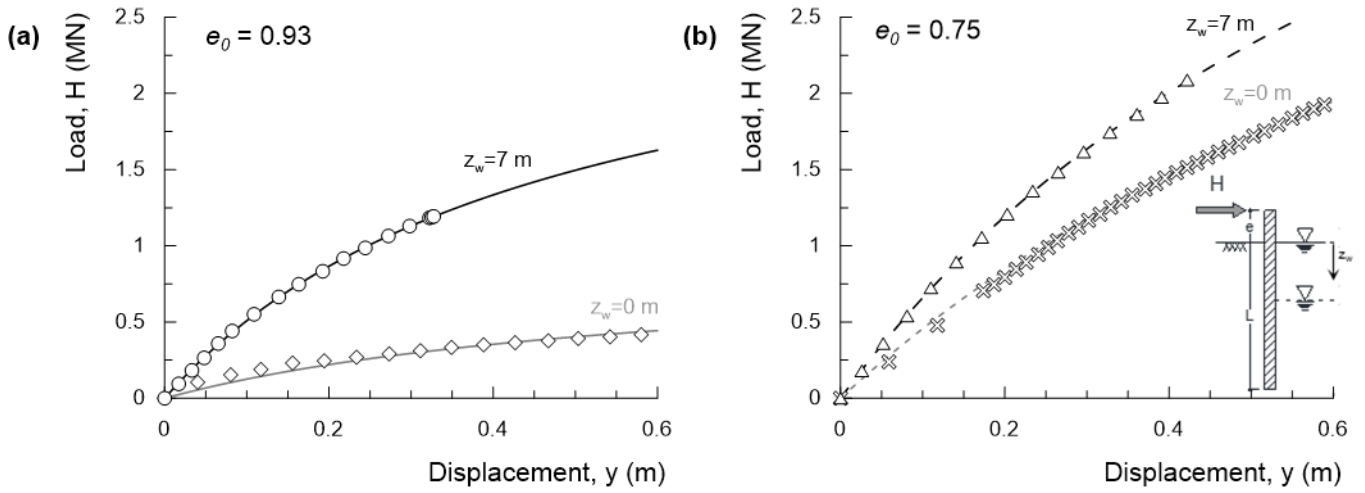


Figure 9: Load-displacement curves: (a) loose soil ( $e_0=0.93$ ), (b) dense soil ( $e_0=0.75$ ).

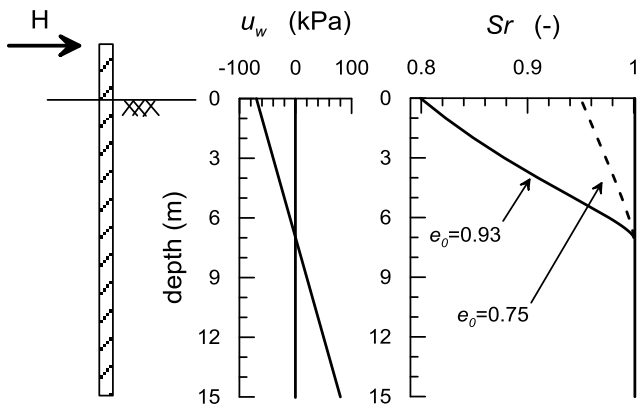


Figure 10: Different distribution of saturation degree due to different porosity for  $z_w=7$  m.

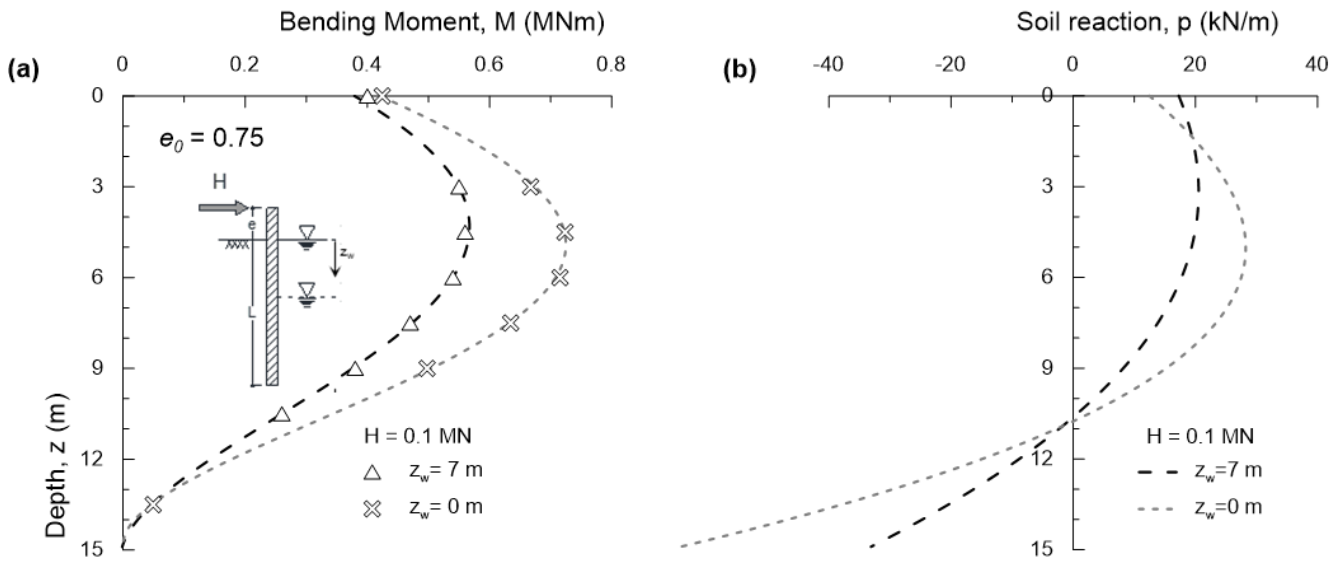
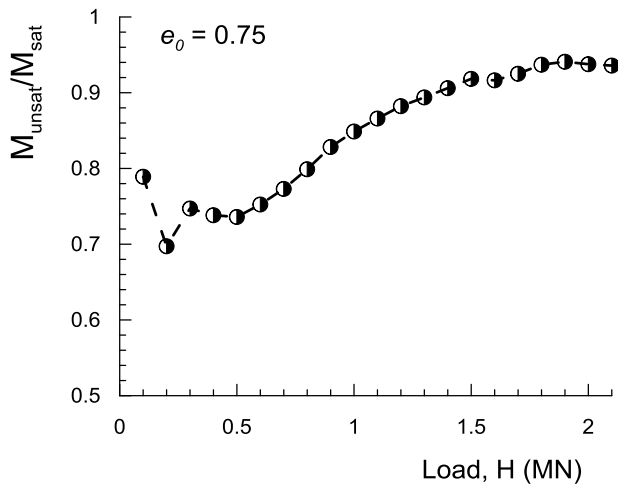


Figure 11: Influence of water table elevation,  $z_w = 0$  (T\_09) and  $z_w = 7$  m (T\_08), for highly compacted soil ( $e_0=0.75$ ): (a) bending moment distribution along pile, (b) soil reaction distribution along pile.

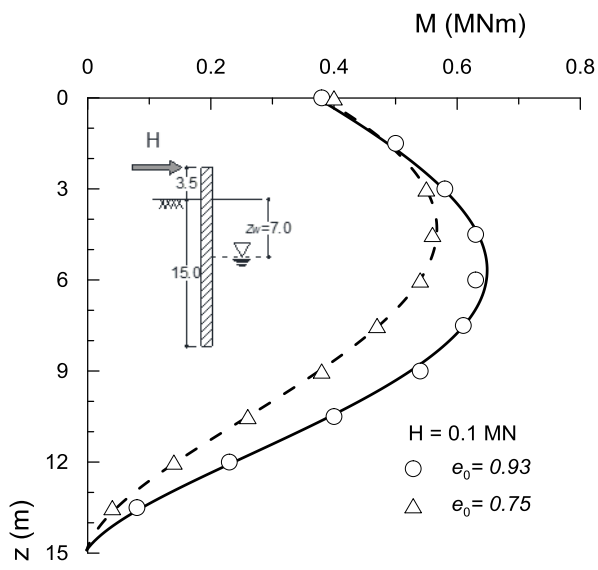


541

542

Figure 12: Maximum bending moment ratio, in unsaturated and saturation condition, for highly compacted soil,  $e_0=0.75$ .

543



544

545

Figure 13: Comparison of bending moment distribution along pile for  $z_w = 7$  m and different initial void ratio.

546

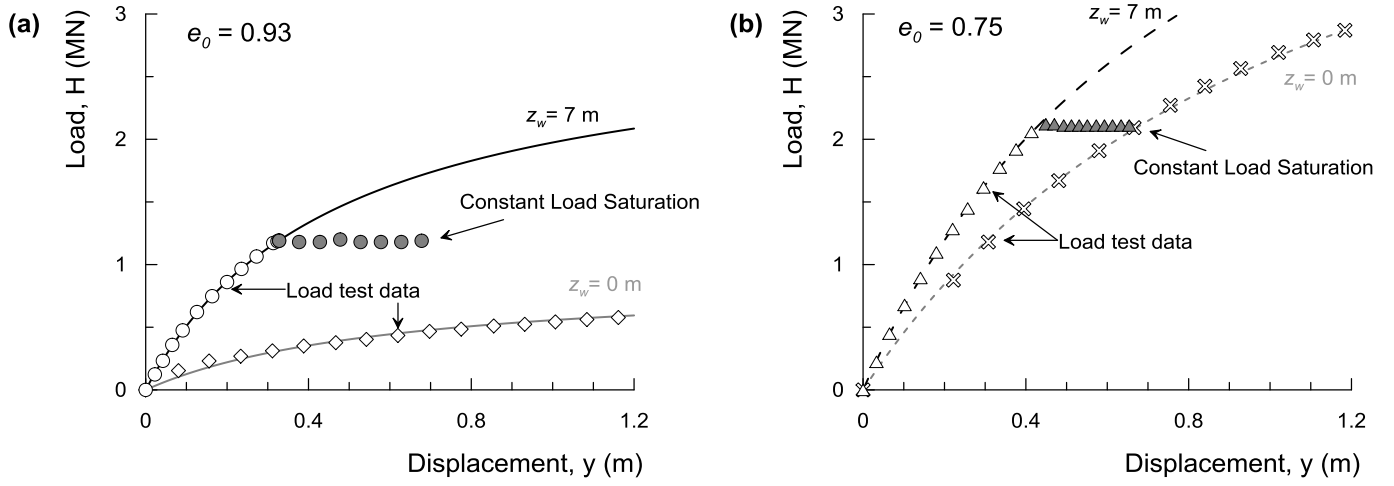


Figure 14: Load-displacement curves during saturation: (a) loose soil ( $e_0=0.93$ ), (b) dense soil ( $e_0=0.75$ ).

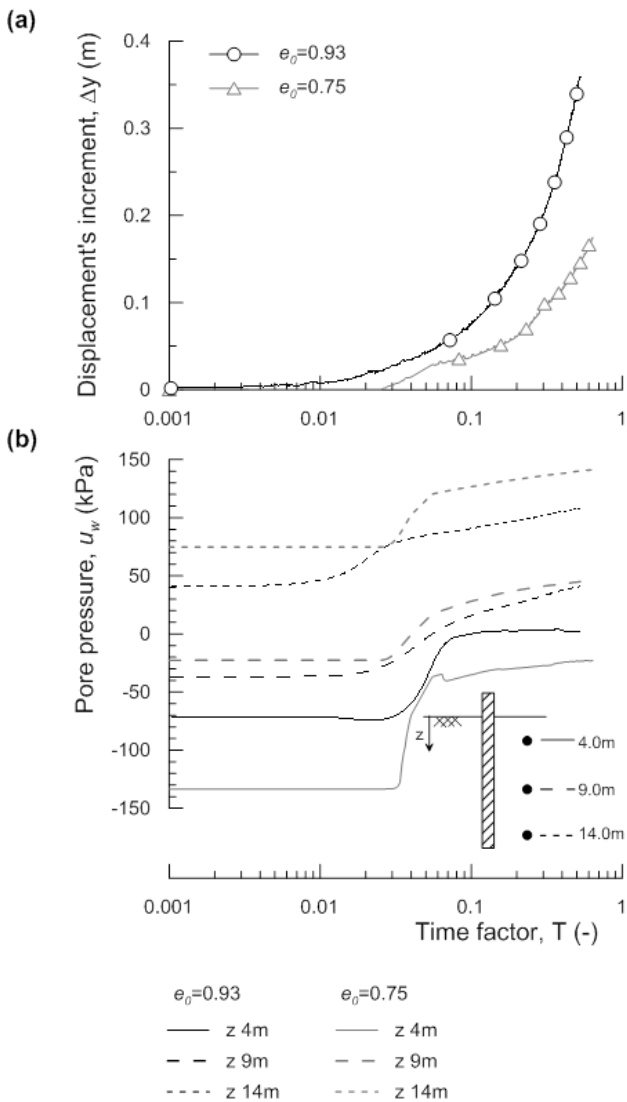


Figure 15: Evolution with time during water table rising of tests T\_06 ( $e_0=0.93$ ) and T\_08 ( $e_0=0.75$ ): (a) lateral displacement, (b) pore pressure at different elevations.

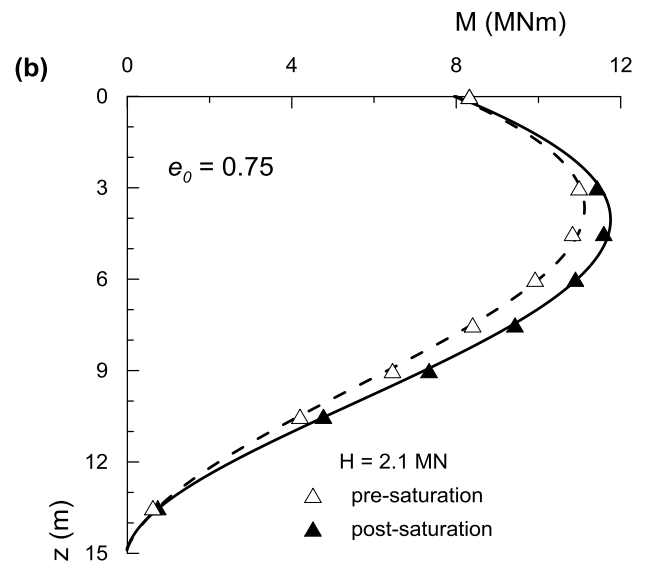
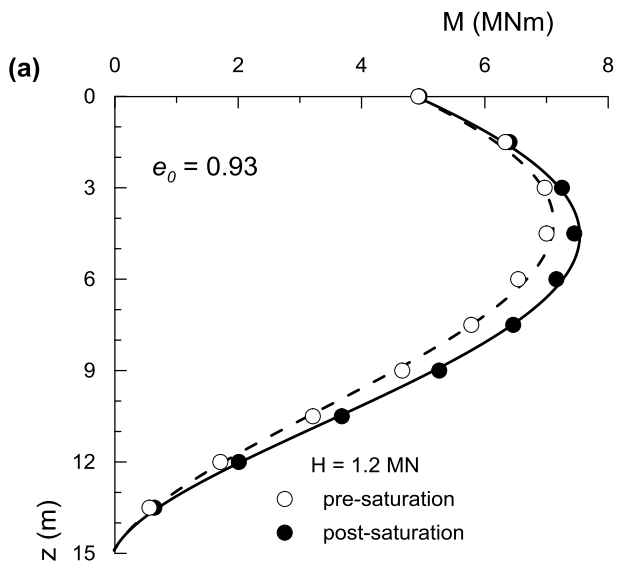


Figure 16: Bending moment profiles before and after saturation: (a) T\_06 ( $e_0=0.93$ ), (b) T\_08 ( $e_0=0.75$ ).